

Novel 3-D Nonstationary MmWave Massive MIMO Channel Models for 5G High-Speed Train Wireless Communications

Yu Liu , Cheng-Xiang Wang , *Fellow, IEEE*, Jie Huang , Jian Sun , *Member, IEEE*, and Wensheng Zhang , *Member, IEEE*

Abstract—In fifth generation (5G) wireless communications, high-speed train (HST) communications is one of the most challenging scenarios. By adopting massive multiple-input multiple-output (MIMO) and millimeter wave (mmWave) technologies into HST communications, the underlying communication system design becomes more challenging and some new channel characteristics have to be studied, such as the non-stationarities in space, time, and frequency domains. This paper proposes a novel three-dimensional space-time-frequency non-stationary mmWave massive MIMO theoretical model, as well as a corresponding simulation model for 5G HST wireless channels based on WINNER II and Saleh–Valenzuela channel models. Cluster evolutions in space, time, and frequency domains are proposed and analyzed to ensure the models’ non-stationarities in three domains. Moreover, based on the proposed channel models, important time-variant channel statistical properties are investigated, such as the time autocorrelation function, space cross-correlation function, delay power spectrum density (PSD), angular PSD, and frequency correlation function. Results indicate that the statistical properties of the simulation model, verified by simulation results, can match well with those of the theoretical model.

Index Terms—5G, HST channels, massive MIMO, mmWave, space-time-frequency non-stationarity.

I. INTRODUCTION

WITH the rapid development of information globalization, wireless communications have penetrated into all aspects of people’s life. Wireless communication systems

have developed from the first to the fourth generations so far. It is expected that by 2020, the fifth generation (5G) wireless communication systems with ultra-high user experience data rate, ultra-high connection density, and ultra-high traffic density will be emerged [1]. As a typical application scenario of 5G communications, high-speed trains (HSTs) received much attention in recent years. Large numbers of HST users demand huge communication data volume, which is far beyond the capacity of current HST communication systems. The widely used Global System for Mobile Communication Railway (GSM-R) is mainly for low-rate train communication and control, and cannot provide personal communications for train users. Then, the Long-Term Evolution Railway (LTE-R) system has been recommended to replace the GSM-R to provide wideband HST communication services [2]. However, in both systems, the HST users communicate directly with the outdoor base stations (BSs). This results in the spotty coverage problem and high penetration losses of wireless signals. HST wireless communication systems also face various challenges, such as frequent handovers, large Doppler spreads, and fast travel through different scenarios. Moreover, the high mobility of trains with a speed of over 500 km/h can make the communication link between the mobile relay station (MRS) and outdoor BS unstable.

To solve the aforementioned problems, some potential 5G technologies, such as massive multiple-input multiple-output (MIMO) and millimeter wave (mmWave), have been considered to provide reliable wideband wireless communication services [3]. Massive MIMO systems can significantly improve the spectrum efficiency and energy efficiency by equipping a large number of antennas at the transmitter (Tx) and/or receiver (Rx) side [4]. MmWave systems cover frequency bands from 30 GHz to 300 GHz and are able to provide large bandwidths in the order of 500 MHz or larger [5]. They can provide high data rate transmissions between MRSs and outdoor BSs. Furthermore, by combining massive MIMO and mmWave technologies, some challenges originating from the high speed of trains and conventional network architectures can be overcome, and the unstable data transmission services can be further improved [6]. For the design, performance evaluation, and test of future HST communication systems assembling massive MIMO and mmWave technologies, an accurate and efficient channel model is essential [7], [8].

Manuscript received March 19, 2018; revised June 3, 2018; accepted July 20, 2018. Date of publication August 21, 2018; date of current version March 14, 2019. This work was supported in part by the National Postdoctoral Program for Innovative Talents (BX201700308), in part by the China Postdoctoral Science Foundation Funded Project (2017M622203), in part by the Natural Science Foundation of China under Grant 61771293, in part by the EU H2020 ITN 5G Wireless Project under Grant 641985, in part by the EU H2020 RISE TESTBED Project under Grant 734325, in part by the Key R&D Program of Shandong Province under Grant 2016GGX101014, in part by the Fundamental Research Funds of Shandong University under Grant 2017JC029, and in part by the Taishan Scholar Program of Shandong Province. The review of this paper was coordinated by the Guest Editors of the Special Issue on Smart Rail Mobility. (Corresponding author: Cheng-Xiang Wang.)

Y. Liu, J. Sun, and W. Zhang are with the Shandong Provincial Key Lab of Wireless Communication Technologies, School of Information Science and Engineering, Shandong University, Shandong 266237, China (e-mail: xinwenliuyu@163.com; sunjian@sdu.edu.cn; zhangwsh@sdu.edu.cn).

C.-X. Wang and J. Huang are with the National Mobile Communications Research Laboratory, Southeast University, Nanjing 210096, China (e-mail: chxwang@seu.edu.cn; hj_1204@sina.cn).

Color versions of one or more of the figures in this paper are available online at <http://ieeexplore.ieee.org>.

Digital Object Identifier 10.1109/TVT.2018.2866414

In the open literature, a variety of HST channel models have been proposed and analyzed to describe various HST communication scenarios [2], [7]–[19]. In [11], a deterministic ray tracing HST channel model was provided to mimic HST tunnel channels, and several channel characteristics, such as frequency selectivity and Doppler spread, were studied. In [12], a three-dimensional (3D) deterministic ray tracing HST tunnel channel model was given, which studied Doppler frequency shift and time delay when two trains met. Ray tracing channel models have high accuracy by incorporating a large amount of channel information but also result in high computational complexity. Both channel models in [11] and [12] adopted the conventional communication architecture that the users inside the train communicate directly with the outdoor BS. In rural macrocell scenario of WINNER II and moving networks of IMT-A channel models, MRSs are deployed. Both channel models introduced the time evolution concept and analyzed the channel non-stationarity. However, the stationary intervals of both models are considerably larger than those of real HST channels measured [13]. Hence, they cannot describe real HST propagation environments precisely. In [14], a two-dimensional (2D) non-stationary geometry-based stochastic model (GBSM) was proposed for HST MIMO channels. All the channel parameters, such as K-factor and propagation distances between the Tx and Rx, are time-variant. Based on the proposed model, some time-variant small-scale fading channel statistical properties, such as autocorrelation function (ACF), space cross-correlation function (CCF), and local scatterer function (LSF), were investigated. Moreover, based on the IMT-A model, a 2D non-stationary HST channel model was proposed in [15]. It assumed that the mobility of both the MRS and clusters results in the channel non-stationarity in the time domain. According to the moving trajectories of clusters and MRS, a series of time-variant small-scale parameters, such as the number of clusters, delays, angle of arrival (AoA), and angle of departure (AoD), were obtained. Then, the channel statistical properties were studied, which were verified by the measurement data. In [16], a 3D non-stationary wideband HST MIMO channel model was proposed based on the WINNER+ channel model. The cluster evolution in time domain was considered, and some key channel statistical properties were investigated. In [17] and [18], the HST channel models for tunnel scenarios were studied. In [19], a novel geometry based random-cluster model for HST channels was presented based on measurement data. The time evolution of the clusters was described by random geometrical parameters. The distributions of these parameters, as well as the path loss, shadow fading, delay, and Doppler spread of each cluster can be extracted from the measurement data. All the above models [2], [9]–[19] focused on HST channels without considering massive MIMO and mmWave technologies.

With more demanding HST communication requirements, some promising 5G technologies such as massive MIMO and mmWave technologies have been considered in HST communication systems to improve the network capacity and the reliability of communication links. In [20], the performance analysis of massive MIMO in HST communications was investigated. The impacts of train speed, K-factor, and signal-to-noise ratio (SNR)

were discussed. It demonstrated that the massive MIMO technology can be applied to HST communications to improve the communication link reliability. Moreover, in [21], a mmWave communication network architecture between the train and BS was presented. A series of simulation results demonstrated the feasibility of mmWave in HST communication systems. Future HST communication systems will develop towards ultra-wideband with mmWave bands and massive MIMO deployment. Accurate channel models that can capture the new channel characteristics are essential and necessary.

For the existing 5G channel models towards standardization, some of them can support high mobility scenarios, such as COST 2100 [22], QuaDRiGa [23], mmMAGIC [24], and 5GCM [25]. COST 2100 channel model [22] can obtain the smooth time evolution and spatial consistency, but cannot support massive MIMO and mmWave. QuaDRiGa model [23] was evolved from the WINNER+ model and can support some new characteristics, such as 3D modeling, massive MIMO, and multi-user and multi-hop networks. However, this model does not support mmWave bands. The mmMAGIC channel model [24] can support larger bandwidth (2 GHz) and wider frequency range (10–80 GHz). It considered high mobility scenarios but no detailed information was given. Based on some 6–100 GHz measurement data and ray tracing results, 5GCM [25] was proposed which considered the HST scenario but cannot support massive MIMO very well. In [7], a general 3D non-stationary 5G channel model was proposed, which can capture small-scale fading channel characteristics of the HST, massive MIMO, and mmWave communication scenarios. It can describe the non-stationarities of the channel in space and time domains, but the frequency non-stationarity was ignored.

To the best of the authors' knowledge, space-time-frequency non-stationary HST channel models considering massive MIMO and mmWave technologies are still missing in the literature. This paper aims to fill the gap. Overall, the major contributions and novelties of this paper are summarized as follows.

- 1) Based on the WINNER II and Saleh-Valenzuela (SV) channel models, a novel space-time-frequency non-stationary massive MIMO and mmWave channel model for HST communications is first proposed. It involves several space-dependent, time-dependent, and frequency-dependent parameters to reflect the effect of massive MIMO and mmWave technologies.
- 2) The corresponding space-time-frequency channel correlation functions are derived and the space-time-frequency evolutions of the proposed channel model are analyzed.
- 3) From the proposed channel model, some statistical properties such as ACF, space CCF, delay power spectrum density (PSD), angular PSD, and frequency correlation function (FCF) are studied.

The remainder of this paper is structured as follows. In Section II, a 3D non-stationary massive MIMO and mmWave channel model for 5G HST communications is presented. Section III analyzes the channel statistical properties. Results and discussions are given in Section IV. Finally, conclusions are drawn in Section V.

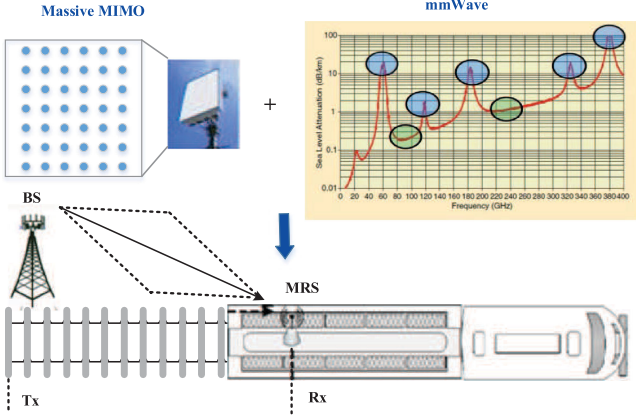


Fig. 1. HST communications network architecture considering massive MIMO and mmWave technologies.

II. NON-STATIONARY MMWAVE MASSIVE MIMO CHANNEL MODELS FOR 5G HST COMMUNICATIONS

A. Description of HST Communication Network Architecture

In this section, a brief description of a HST network considering massive MIMO and mmWave technologies is provided. It adopts a two-tiered network architecture to separate the indoor and outdoor channels [14]. In outdoor channels, at least one MRS is deployed on the top of each carriage, which can establish a communication link with the indoor users and transfer all the communication data inside train to the outdoor BS.

MRSs are deployed on the surface of train to improve the quality of received signal, and mitigate high penetration losses of signals traveling into train carriages. The massive MIMO technology is adopted to improve the spectrum efficiency and energy efficiency by installing large number of antennas at the BS and/or MRS [26], [27]. Moreover, for the outdoor communications between the MRS and BS, the mmWave technology is considered. The mmWave communications can bring huge bandwidth and achieve high data transmission rate [5]. All these technologies can be applied to increase communication capacity and improve system performance. The HST communication network architecture considering the MRS, massive MIMO, and mmWave is illustrated in Fig. 1.

B. The Massive MIMO and MmWave Channel Model for HST Communications

Let us consider a massive MIMO system with P and Q antenna elements at Tx (BS) side and Rx (MRS) side, respectively. The carrier frequency is denoted by f_c . By taking the elevation angles into consideration, a 3D twin-cluster model is considered [7]. The corresponding channel model framework is shown in Fig. 2. For clarity, only the n th cluster pair ($n = 1, 2, \dots, N$) is illustrated, where N is the number of clusters. Each sphere in the figure with several dots represents a cluster, which can be moving or static with certain probability. Moreover, clusters are randomly distributed in pairs. The n th twin-cluster can be denoted by $C_{n,A}$ and $C_{n,Z}$. Here, $C_{n,A}$ is a representation of the first bounce at the Tx side and $C_{n,Z}$ is a representation

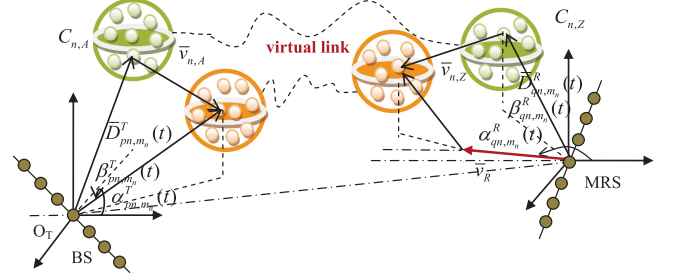


Fig. 2. A 3D non-stationary twin-cluster HST channel model.

of the last bounce at Rx side. The propagation space between the two clusters can be abstracted as a virtual link [16]. The inter-element spacings at the Tx and Rx are denoted by Δx_T and Δx_R , respectively. It is assumed that the Tx is fixed and Rx is in motion. The movement of the Rx can be denoted by a velocity vector \bar{v}_R with speed v_R . The velocity vector of $C_{n,A}$ is denoted by $\bar{v}_{n,A}$ with speed $v_{n,A}$ and the velocity vector of $C_{n,Z}$ is denoted by $\bar{v}_{n,Z}$ with speed $v_{n,Z}$. It should be noted that all the parameters are established as time-variant.

1) *The Theoretical Model:* Based on the WINNER II and SV channel models, the non-stationary space-time-frequency HST channel model considering massive MIMO and mmWave technologies is proposed. The complex channel transfer function (CTF) consists of the line-of-sight (LoS) and non-LoS (NLoS) components. The theoretical channel model can be expressed as [7]

$$H_{pq}(t, f) = H_{pq}^{\text{LoS}}(t, f) + \lim_{M_n \rightarrow \infty} \sum_{n=1}^{N(t)} \sum_{m_n=1}^{M_n} H_{pq,n,m_n}^{\text{NLoS}}(t, f) \quad (1)$$

–In the LoS case

$$H_{pq}^{\text{LoS}}(t, f) = \begin{bmatrix} F_{p,V}^T(\alpha_{\text{LoS}}^T(t), \beta_{\text{LoS}}^T(t)) \\ F_{p,H}^T(\alpha_{\text{LoS}}^T(t), \beta_{\text{LoS}}^T(t)) \end{bmatrix}^T \begin{bmatrix} e^{j\Theta_{\text{LoS}}^{VV}} & 0 \\ 0 & e^{j\Theta_{\text{LoS}}^{HH}} \end{bmatrix} \begin{bmatrix} F_{q,V}^R(\alpha_{\text{LoS}}^R(t), \beta_{\text{LoS}}^R(t)) \\ F_{q,H}^R(\alpha_{\text{LoS}}^R(t), \beta_{\text{LoS}}^R(t)) \end{bmatrix} \sqrt{\frac{K_{pq}(t)}{K_{pq}(t) + 1}} e^{-j2\pi \frac{\bar{D}_{pq}^{\text{LoS}}(t)}{\lambda}} \times e^{j2\pi f_{pq}^{\text{LoS}}(t) \cdot t} \cdot e^{-j2\pi f \cdot \tau_{pq}^{\text{LoS}}(t)}. \quad (2)$$

For the LoS component, $\alpha_{\text{LoS}}^T(t)$ and $\beta_{\text{LoS}}^T(t)$ denote the azimuth angle of departure (AAoD) and the elevation angle of departure (EAoD) between the center of Tx array and Cluster $C_{n,A}$, respectively. $\alpha_{\text{LoS}}^R(t)$ and $\beta_{\text{LoS}}^R(t)$ denote the azimuth angle of arrival (AAoA) and the elevation angle of arrival (EAoA) between the center of Cluster $C_{n,Z}$ and Rx array, respectively. $f_{pq}^{\text{LoS}}(t)$ is the Doppler frequency of LoS. $\tau_{pq}^{\text{LoS}}(t)$ is the LoS delay between the Tx and Rx, and $K_{pq}(t)$ is the K-factor. Here, V and H denote vertical polarization and horizontal polarization, respectively. Θ_{LoS}^{VV} and Θ_{LoS}^{HH} are the initial phases, which follow the uniform distribution over the $(0, 2\pi)$. Functions $F_V^T(\cdot)$, $F_H^T(\cdot)$, $F_V^R(\cdot)$, and $F_H^R(\cdot)$ denote the antenna patterns in the global coordinate system (GCS) with the origin at the center of Tx array.

–In the NLoS case

$$\begin{aligned}
 H_{pq,n,m_n}^{\text{NLoS}}(t, f) &= \begin{bmatrix} F_{p,V}^T(\alpha_{pn,m_n}^T(t), \beta_{pn,m_n}^T(t)) \\ F_{p,H}^T(\alpha_{pn,m_n}^T(t), \beta_{pn,m_n}^T(t)) \end{bmatrix}^T \\
 &\begin{bmatrix} \sqrt{\kappa_{n,m_n}^{-1}} e^{j\Theta_{n,m_n}^{VV}} & e^{j\Theta_{n,m_n}^{VH}} \\ e^{j\Theta_{n,m_n}^{HV}} & \sqrt{\kappa_{n,m_n}^{-1}} e^{j\Theta_{n,m_n}^{HH}} \end{bmatrix} \\
 &\begin{bmatrix} F_{q,V}^R(\alpha_{qn,m_n}^R(t), \beta_{qn,m_n}^R(t)) \\ F_{q,H}^R(\alpha_{qn,m_n}^R(t), \beta_{qn,m_n}^R(t)) \end{bmatrix} \cdot \sqrt{\frac{P_{n,m_n}(t)}{K_{pq}(t) + 1}} \cdot \left(\frac{f}{f_c}\right)^{r_{n,m_n}} \\
 &\times e^{j\left(\varphi_{n,m_n} - 2\pi \frac{\bar{D}_{pq,n,m_n}^T(t)}{\lambda}\right)} \cdot e^{j2\pi f_{pq,n,m_n}(t) \cdot t} \\
 &\times e^{-j2\pi f \cdot (\tau_{pq,n}(t) + \tau_{pq,n,m_n}(t))}. \quad (3)
 \end{aligned}$$

For the NLoS component, $N(t)$ is the time-variant cluster number. M_n is the ray number within n th cluster, $\tau_{pq,n}(t)$ is the delay between the p th Tx antenna and q th Rx antenna via n th cluster, $\tau_{pq,n,m_n}(t)$ is the relative delay between the p th Tx antenna and q th Rx antenna via the m_n th ray with n th cluster, and κ_{n,m_n} is the cross polarization power ratio. Here, Θ_{n,m_n}^{VV} , Θ_{n,m_n}^{VH} , Θ_{n,m_n}^{HV} , and Θ_{n,m_n}^{HH} are the initial random phases of the m_n th ray of the n th cluster in four polarization directions. It should be noted that the phases follow the uniform distribution within $(0, 2\pi)$ and r_{n,m_n} is the frequency-dependent factor [28]. In the proposed HST channel model, all the parameters are time-variant. Moreover, the massive MIMO technology will bring spherical wavefront and cluster birth-death process along the antenna array axis. The mmWave will introduce the appearance and disappearance of clusters in the frequency domain. The channel will exhibit non-stationarities in space, time, and frequency domains. Our proposed channel model has the capability to model the space-time-frequency non-stationarities of HST channels. The Doppler frequency $f_{pq,n,m_n}(t)$ can be shown as

$$\begin{aligned}
 f_{pq,n,m_n}(t) &= f_{pn,m_n}^T(t) + f_{qn,m_n}^R(t) \\
 &= \frac{(\bar{v}_R - \bar{v}_{n,Z}) \cdot \bar{\phi}_{qn,m_n}^R(t) - \bar{v}_{n,A} \bar{\phi}_{pn,m_n}^T(t)}{\lambda}. \quad (4)
 \end{aligned}$$

It should be noted that the Doppler frequency $f_{pq,n,m_n}(t)$ is caused by the movement of Cluster $C_{n,A}$, Cluster $C_{n,Z}$, and MRS. The wavelength is $\lambda = c/f_c$. Moreover, the velocity vectors of Cluster $C_{n,A}$, Cluster $C_{n,Z}$, and MRS can be expressed as

$$\bar{v}_{n,A} = v_{n,A} \cdot \begin{bmatrix} \cos \varphi_{n,A} \cdot \cos \vartheta_{n,A} \\ \cos \varphi_{n,A} \cdot \sin \vartheta_{n,A} \\ \sin \varphi_{n,A} \end{bmatrix}^T \quad (5)$$

$$\bar{v}_{n,Z} = v_{n,Z} \cdot \begin{bmatrix} \cos \varphi_{n,Z} \cdot \cos \vartheta_{n,Z} \\ \cos \varphi_{n,Z} \cdot \sin \vartheta_{n,Z} \\ \sin \varphi_{n,Z} \end{bmatrix}^T \quad (6)$$

$$\bar{v}_R = v_R \cdot \begin{bmatrix} \cos \varphi_R \cdot \cos \vartheta_R \\ \cos \varphi_R \cdot \sin \vartheta_R \\ \sin \varphi_R \end{bmatrix}^T. \quad (7)$$

The 3D AoD vectors between the p th Tx array element and m_n th ray of Cluster $C_{n,A}$ can be expressed as

$$\bar{\phi}_{pn,m_n}^T(t) = \begin{bmatrix} \cos \beta_{pn,m_n}^T(t) \cdot \cos \alpha_{pn,m_n}^T(t) \\ \cos \beta_{pn,m_n}^T(t) \cdot \sin \alpha_{pn,m_n}^T(t) \\ \sin \beta_{pn,m_n}^T(t) \end{bmatrix}^T. \quad (8)$$

The AoA vectors between the m_n th ray of Cluster $C_{n,Z}$ and the q th Rx array element can be expressed as

$$\bar{\phi}_{qn,m_n}^R(t) = \begin{bmatrix} \cos \beta_{qn,m_n}^R(t) \cdot \cos \alpha_{qn,m_n}^R(t) \\ \cos \beta_{qn,m_n}^R(t) \cdot \sin \alpha_{qn,m_n}^R(t) \\ \sin \beta_{qn,m_n}^R(t) \end{bmatrix}^T. \quad (9)$$

Moreover, the delay between the p th Tx and q th Rx via m_n th ray of n th cluster consists of the delay of first bounce, the delay of last bounce, and the virtual link delay $\tilde{\tau}_{pq,n,m_n}(t)$. The total delay can be expressed as

$$\begin{aligned}
 \tau_{pq,n,m_n}(t) &= \frac{\|\bar{D}_{pq,n,m_n}^T(t)\|}{c} + \tilde{\tau}_{pq,n,m_n}(t) \\
 &= \frac{[\|\bar{D}_{pn,m_n}^T(t)\| + \|\bar{D}_{qn,m_n}^R(t)\|]}{c} + \tilde{\tau}_{pq,n,m_n}(t). \quad (10)
 \end{aligned}$$

The distance between the p th Tx and m_n th ray in Cluster $C_{n,A}$ can be expressed as

$$\bar{D}_{pn,m_n}^T(t) = \bar{D}_{pn,m_n}^T(t_0) + \bar{v}_{n,A} \cdot t \quad (11)$$

$$\bar{D}_{pn,m_n}^T(t_0) = \bar{D}_{pn,m_n}^T(t_0) \cdot \bar{\phi}_{pn,m_n}^T(t_0). \quad (12)$$

The distance between the m_n th ray in Cluster $C_{n,Z}$ and q th Rx can be expressed as

$$\bar{D}_{qn,m_n}^R(t) = \bar{D}_{qn,m_n}^R(t_0) + \bar{v}_{n,Z} \cdot t \quad (13)$$

$$\bar{D}_{qn,m_n}^R(t_0) = \bar{D}_{qn,m_n}^R(t_0) \cdot \bar{\phi}_{qn,m_n}^R(t_0). \quad (14)$$

The mean power of m_n rays within n th cluster can be obtained by

$$P_{n,m_n}(t) = e^{\frac{(-\tau_{n,m_n}(t))(\chi-1)}{E[\tau_{n,m_n}(t)]}} \cdot 10^{-\frac{Z_{n,m_n}}{10}} \quad (15)$$

where χ denotes the delay scaling parameters, $E[\tau_{n,m_n}(t)]$ is the mean relative delay via the m_n th ray of the n th cluster, and Z_{n,m_n} is the shadowing of each ray per cluster following a Gaussian distribution.

The generation process of the space-time-frequency non-stationary 5G HST channel model is shown in Fig. 3. It takes the array, time, and frequency evolutions into consideration. All the aforementioned parameters are listed as Table I.

TABLE I
DEFINITION OF PARAMETERS

Parameters	Definition
$\alpha_{\text{LoS}}^T(t), \beta_{\text{LoS}}^T(t)$	AAoD and EAoD in the LoS case, respectively
$\alpha_{\text{LoS}}^R(t), \beta_{\text{LoS}}^R(t)$	AAoA and EAoA in the LoS case, respectively
$f_{pq}^{\text{LoS}}(t)$	Doppler frequency of the LoS case between the p th Tx and the q th Rx
$f_{pn,m_n}^T(t), f_{qn,m_n}^R(t)$	Doppler frequencies of the p th Tx (q th Rx) via the m_n th ray of the n th cluster
$P_{n,m_n}(t)$	Mean power of the m_n th ray of the n th cluster
$\bar{\mathbf{v}}_R$	3D velocity vector of Rx array
$\bar{\mathbf{v}}_{n,A}, \bar{\mathbf{v}}_{n,Z}$	3D velocity vectors of Cluster $C_{n,A}$ and Cluster $C_{n,Z}$, respectively
$\alpha_{pn,m_n}^T(t), \beta_{pn,m_n}^T(t)$	AAoD and EAoD of the Tx via the m_n th ray of the n th cluster in the NLoS case, respectively
$\alpha_{qn,m_n}^R(t), \beta_{qn,m_n}^R(t)$	AAoA and EAoA of the Rx via the m_n th ray of the n th cluster in the NLoS case, respectively
$\varphi_{n,A}, \vartheta_{n,A}$	Azimuth and elevation angles of Cluster $C_{n,A}$, respectively
$\varphi_{n,Z}, \vartheta_{n,Z}$	Azimuth and elevation angles of Cluster $C_{n,Z}$, respectively
φ_R, ϑ_R	Azimuth and elevation angles of Rx array, respectively
$D_{pq}^{\text{LoS}}(t)$	Distance between the p th Tx and the q th Rx
$D_{pq,n,m_n}^{\text{LoS}}(t)$	Distance between the p th Tx and the q th Rx via the m_n th ray with the n th cluster
$D_{pn,m_n}^T(t)$	Distance between the p th Tx and the n th cluster via the m_n th ray
$D_{qn,m_n}^R(t)$	Distance between the n th cluster via the m_n th ray and the q th Rx
$\tau_{pq}^{\text{LoS}}(t)$	LoS delay between the p th Tx antenna and the q th Rx antenna
$\tau_{pq,n}(t)$	Delay between the p th Tx antenna and the q th Rx antenna via the n th cluster
$\tau_{pq,n,m_n}(t)$	Delay between the p th Tx antenna and the q th Rx antenna via the m_n th ray with the n th cluster
$\tilde{\tau}_{pq,n,m_n}(t)$	Delay of virtual link
$K_{pq}(t)$	Rice K-factor
$N(t)$	Number of observable clusters
$M_n(t)$	Number of rays within the n th cluster
λ_G, λ_R	Generation rate and recombination rate of cluster, respectively

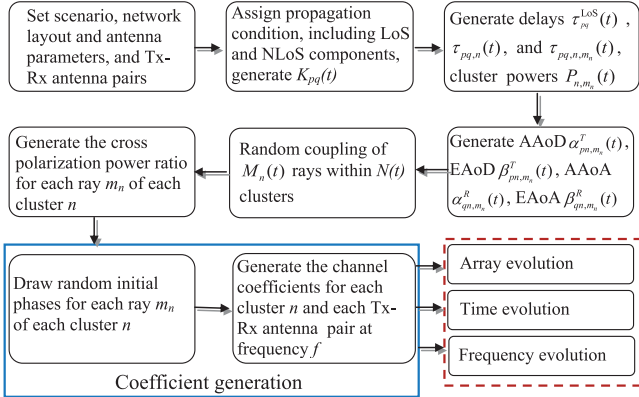


Fig. 3. The generation process of the HST channel model.

2) *The Simulation Model*: Based on the proposed theoretical HST channel model, the simulation model can be developed by using the discrete angles. Here, the method of equal area (MEA) is used to obtain the discrete AAoDs, EAoDs, AAoAs, and EAoAs. The simulation model can be expressed as

$$\tilde{H}_{pq}(t, f) = \tilde{H}_{pq}^{\text{LoS}}(t, f) + \sum_{n=1}^{N(t)} \sum_{m_n=1}^{M_n} \tilde{H}_{pq,n,m_n}^{\text{NLoS}}(t, f). \quad (16)$$

C. Cluster Evolution in Space, Time, and Frequency Domains for HST Channel Model

The non-stationarities of our proposed HST channel model result from two mechanisms, i.e., the time-variant parameters and the birth-death process of clusters in space/time/frequency axes. The clusters in a specific HST scenario can exist over a certain time period [2]. During this period, the number of

clusters can be seen as unchanged. When it is over the period, some of previous clusters disappear and some new clusters appear [7]. In this section, the space, time, and frequency cluster evolutions for the proposed HST channel model are developed, as shown in Fig. 4. The flowchart in Fig. 4 can be described in details as follows.

Firstly, a series of initial cluster sets are generated at time t [16]. Some parameters, such as number of rays in a cluster, delays of rays, power, angular parameters, and virtual link delay, need to be assigned. These parameters are generated randomly and different parameters follow different distributions. The number of rays follow a Poisson distribution. The virtual link delays of clusters and the delays of rays are assumed to follow exponential distributions. Moreover, the angular parameters, such as AAoAs, AAoDs, EAoAs, and EAoDs, are assumed to be wrapped Gaussian distributions [7].

Secondly, to describe the cluster evolution more accurately, two types of sampling intervals can be used in the evolution process [16]. The first type is the channel sampling intervals, such as Δi in space (antenna array) domain, Δt in time domain, and Δf in frequency domain. The channel parameters should be updated continuously during these periods. The other type of sampling intervals are the periods in which the clusters are needed to be updated. These intervals can be described by Δi_e , Δt_e , and Δf_e . During Δi_e , Δt_e , and Δf_e , the birth and death of clusters occur. Here, we take the cluster evolution in time domain as an example. For the proposed channel model, it will generate some clusters initially. These clusters can be updated during the aforementioned sampling intervals. Some of these clusters disappear and others survive. Moreover, some new clusters appear. Each cluster has its own survival probability $P_{\text{surv}}(\Delta t_e)$, which is calculated by the relative velocities of clusters. By extending time domain to space-time-frequency domain, the survival

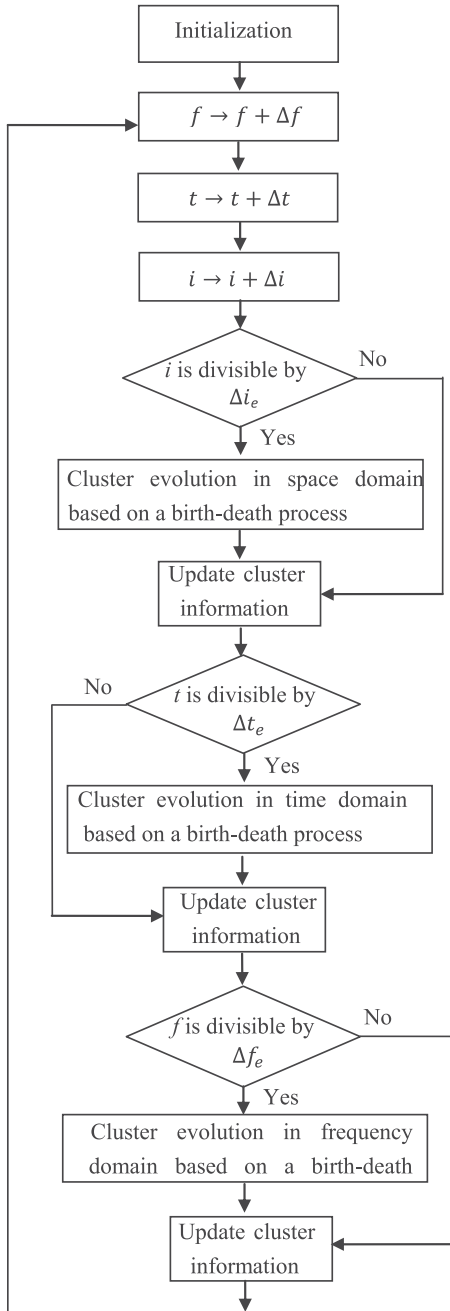


Fig. 4. The flowchart of space-time-frequency cluster evolution of the proposed HST channel model.

probability of a cluster in the proposed space-time-frequency channel model should consist of three parts. The final survival probability is jointly influenced by space, time, and frequency domains, which can be calculated as

$$\begin{aligned}
 & P_{surv}(\Delta i_e, \Delta t_e, \Delta f_e) \\
 &= P_{surv}(\Delta i_e) \cdot P_{surv}(\Delta t_e) \cdot P_{surv}(\Delta f_e) \\
 &= e^{-\lambda_R \cdot \frac{A(p, q, p', q', \Delta i_e)}{D_i}} \cdot e^{-\lambda_R \cdot \frac{T(\bar{v}_R, \Delta t_e)}{D_t}} \cdot e^{-\lambda_R \cdot \frac{F(\Delta f_e)}{D_f}}. \quad (17)
 \end{aligned}$$

Note that D_i , D_t , D_f , and $F(\Delta f_e)$ can be determined by channel measurements. Meanwhile, a lot of new clusters need to

be generated. Let us assume that the birth rate is λ_G and the death rate is λ_R . The number of newly generated clusters can be expressed as

$$\begin{aligned}
 & E[N_{ng}(i + \Delta i_e, t + \Delta t_e, f + \Delta f_e)] \\
 &= \frac{\lambda_G}{\lambda_R} (1 - P_{surv}(\Delta i_e, \Delta t_e, \Delta f_e)). \quad (18)
 \end{aligned}$$

Thirdly, the newly generated clusters and the survival clusters need to be updated. For the newly generated clusters, some parameters such as delay, power, and angular parameters are assigned randomly just as the initialization process. For the survival clusters, the corresponding delay, power, and angular parameters are updated from the previous time instant. Following the steps above, the space-time-frequency non-stationarity of the channel model can be guaranteed.

III. STATISTICAL PROPERTIES ANALYSIS

In this section, we will derive typical statistical properties of the proposed non-stationary simulation HST channel model.

A. The Delay PSD

The time-variant delay PSD $\Upsilon(t, \tau_{pq})$ of channel between the p th Tx antenna and the q th Rx antenna can be expressed as

$$\begin{aligned}
 \Upsilon(t, \tau_{pq}) &= \sum_{n=1}^{N(t)} \sum_{m_n=1}^{M_n} |h_{pq, n, m_n}(t)|^2 \\
 &\quad \times \delta(\tau_{pq} - \tau_{pq, n}(t) - \tau_{pq, n, m_n}(t)). \quad (19)
 \end{aligned}$$

The time-variant delay PSD is influenced by the time-dependent mean powers of rays with clusters and delays of rays parameters. The cluster power can be obtained from the channel impulse response (CIR) $h_{pq, n, m_n}(t)$, which is the inverse Fourier transform of CTF. All these parameters are related to the continuously updated geometrical relationship.

B. Space-Time-Frequency Correlation Function

The correlation function of two arbitrary CTF of $\tilde{H}_{pq}(t, f)$ and $\tilde{H}_{p'q'}^*(t, f)$ can be defined as the summation of all the clusters with no inter-correlation. To investigate the correlation properties, the space-time-frequency correlation function $R_H(\Delta t, \Delta f, \Delta x_T, \Delta x_R)$ can be calculated as

$$\begin{aligned}
 & R_H(\Delta t, \Delta f, \Delta x_T, \Delta x_R) \\
 &= E[\tilde{H}_{pq}(t, f) \cdot \tilde{H}_{p'q'}^*(t - \Delta t, f - \Delta f)] \\
 &= R_H^{\text{LoS}}(\Delta t, \Delta f, \Delta x_T, \Delta x_R) + R_H^{\text{NLoS}}(\Delta t, \Delta f, \Delta x_T, \Delta x_R) \quad (20)
 \end{aligned}$$

where $E[\cdot]$ denotes the expectation operator, and $(\cdot)^*$ denotes the complex conjugate operation. The propagation channel consists of two parts: the LoS and NLoS components. The LoS component is calculated by the locations of the Tx and Rx. The NLoS components are generated randomly. Assuming that the LoS and NLoS components are independent with each other, (20) can be expressed as the summation of LoS component

correlation and NLoS components correlation. The detailed space-time-frequency correlation function $R_H^{\text{LoS}}(\Delta t, \Delta f, \Delta x_T, \Delta x_R)$ and $R_H^{\text{NLoS}}(\Delta t, \Delta f, \Delta x_T, \Delta x_R)$ can be rewritten as

$$\begin{aligned} \text{--In the LoS case,} \\ R_H^{\text{LoS}}(\Delta t, \Delta f, \Delta x_T, \Delta x_R) &= \frac{K_{pq}(t)}{K_{pq}(t) + 1} \tilde{H}_{pq}^{\text{LoS}}(t, f) \\ &\quad \cdot \tilde{H}_{p'q'}^{\text{LoS}*}(t - \Delta t, f - \Delta f) \end{aligned} \quad (21)$$

–In the NLoS case,

$$\begin{aligned} R_H^{\text{NLoS}}(\Delta t, \Delta f, \Delta x_T, \Delta x_R) \\ = \frac{1}{K_{pq}(t) + 1} \sum_{n=1}^{N(t)} \sum_{m_n=1}^{M_n} \tilde{H}_{pq,n,m_n}^{\text{NLoS}}(t, f) \\ \cdot \tilde{H}_{p'q',n,m_n}^{\text{NLoS}*}(t - \Delta t, f - \Delta f). \end{aligned} \quad (22)$$

According to the above equations, the time-variant space CCF can be obtained by imposing $\Delta t = 0$ and $\Delta f = 0$ in (20) and can be expressed as

$$\begin{aligned} \rho_H(\Delta x_T, \Delta x_R) &= R_H(\Delta x_T, \Delta x_R, 0, 0) \\ &= \rho_H^{\text{LoS}}(\Delta x_T, \Delta x_R) + \rho_H^{\text{NLoS}}(\Delta x_T, \Delta x_R). \end{aligned} \quad (23)$$

By setting Δx_T , Δx_R , and Δf in (20) as 0, the space-time-frequency correlation function can be reduced as the time-variant ACF, which can be expressed as

$$r_H(\Delta t) = R_H(\Delta t, 0, 0, 0) = r_H^{\text{LoS}}(\Delta t) + r_H^{\text{NLoS}}(\Delta t). \quad (24)$$

C. The FCF

By setting Δx_T , Δx_R , and Δt in (20) as 0, the time-variant frequency correlation function (FCF) can be obtained, which can be expressed as

$$\begin{aligned} \kappa_H(t, \Delta f) &= E \left[\tilde{H}_{pq}(t, f) \cdot \tilde{H}_{pq}^*(t, f - \Delta f) \right] \\ &= R_H(\Delta f, 0, 0, 0) = \kappa_H^{\text{LoS}}(t, \Delta f) + \kappa_H^{\text{NLoS}}(t, \Delta f). \end{aligned} \quad (25)$$

D. The Doppler PSD

By taking the Fourier transform of ACF with respect to Δt , the time-variant Doppler PSD can be obtained, which can be illustrated as

$$\begin{aligned} \tilde{S}_H(t, f_D) &= \int_{-\infty}^{\infty} r_H(\Delta t) e^{-j2\pi f_D \Delta t} d\Delta t \\ &= \int_{-\infty}^{\infty} (r_H^{\text{LoS}}(\Delta t) + r_H^{\text{NLoS}}(\Delta t)) \cdot e^{-j2\pi f_D \Delta t} d\Delta t. \end{aligned} \quad (26)$$

E. The Angular PSD

The time-variant angular PSD $\Lambda(t, \Omega)$ of channel can be acquired by the CIR $h_{pq,n,m_n}(t)$. It describes the distribution of power spectrum in the angular domain, which can be

expressed as

$$\Lambda(t, \Omega) = \sum_{n=1}^{N(t)} \sum_{m_n=1}^{M_n} |h_{pq,n,m_n}(t)|^2 \delta(\Omega - \Omega_{pq,n} - \Omega_{pq,n,m_n}) \quad (27)$$

where Ω denotes the AoAs or AoDs, $\Omega_{pq,n}$ is the mean angle of the n th cluster, and Ω_{pq,n,m_n} is the angle offset of the m_n th ray in the n th cluster.

F. The Stationary Intervals in Space-Time-Frequency Domain

The stationary interval is the period during which the channel can be seen as unchanged compared with the neighbor channel. To obtain the stationary interval in space-time-frequency domain, the time-variant correlation matrix distance (CMD) can be applied [29]. The CMD can be calculated in space-time-frequency domain as follows

$$\begin{aligned} d_{corr}(\Delta t_s, \Delta f_s, \Delta i_s) \\ = 1 - \frac{\text{tr}\{R_H(t; f; i)R_H(t + \Delta t_s; f + \Delta f_s; i + \Delta i_s)\}}{\|R_H(t; f; i)\|_F \|R_H(t + \Delta t_s; f + \Delta f_s; i + \Delta i_s)\|_F} \end{aligned} \quad (28)$$

where $R_H(t; f; i)$ is the correlation function of channel transfer function. Δt_s is the time stationary interval, Δf_s is the frequency stationary, and Δi_s is the space stationary interval. The above stationary intervals can be used to evaluate the non-stationary behaviors of HST channels in space/time/frequency domains.

IV. RESULTS AND DISCUSSIONS

In this part, the statistical properties of the proposed HST channel models are studied and analyzed. The related simulation parameters are listed as follows. The generation rate $\lambda_G = 80/\text{m}$, and the recombination rate $\lambda_R = 4/\text{m}$. The moving speed of MRS is $v_R = 100 \text{ m/s}$, and the BS is fixed. The moving speeds of $C_{n,A}$ and $C_{n,Z}$ are selected as $v_{n,A} = 30 \text{ m/s}$ and $v_{n,Z} = 30 \text{ m/s}$, respectively. The carrier frequency is set as $f_c = 58 \text{ GHz}$, and the antenna elements at Tx and Rx are both set as 32. The number of rays in each cluster is set as 20. The percentage of moving clusters is $P_F = 0.3$ [30]. The initial AAoD $\varphi_{n,A}$ and EAoD $\vartheta_{n,A}$ of the n th twin cluster at the Tx side are $\varphi_{n,A} = \frac{\pi}{3}$, $\vartheta_{n,A} = \frac{\pi}{4}$. Moreover, the initial AAoA $\varphi_{n,Z}$ and EAoA $\vartheta_{n,Z}$ of the n th twin cluster at the Rx side are $\varphi_{n,Z} = \frac{\pi}{3}$, $\vartheta_{n,Z} = \frac{\pi}{4}$. All the angular parameters are randomly generated by the Gaussian distribution. The initial distance between the p th Tx antenna element and m_n th ray of n th cluster $C_{n,A}$ is $D_{pn,m_n}^T(t_0) = 50 \text{ m}$, and the initial distance between the m_n th ray of n th cluster $C_{n,Z}$ and q th Rx antenna element is $D_{qn,m_n}^R(t_0) = 100 \text{ m}$. The length of railway between the Tx and Rx is set as $D = 200 \text{ m}$ [14]. All the simulations are conducted in the NLoS case. The rest parameters are randomly generated refer to the WINNER II channel model [31]. The MEA is employed to obtain the discrete AoA and AoD angular parameters, respectively. The k value of the von Mises distribution is selected as 6.

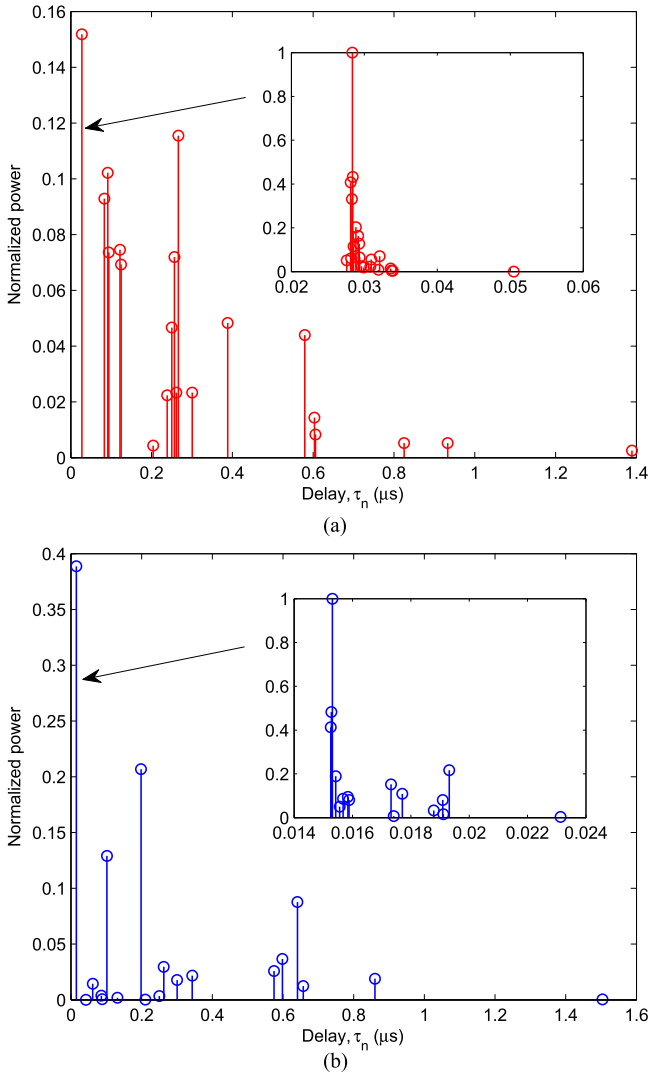


Fig. 5. The delay PSDs of the non-stationary HST simulation channel model at (a) $t = 2$ s and (b) $t = 4$ s ($D_{p_n, m_n}^T(t_0) = 50$ m, $D_{q_n, m_n}^R(t_0) = 100$ m, $\lambda_G = 80$ m, $\lambda_R = 4$ m, $v_{n,A} = 30$ m/s, $v_{n,Z} = 30$ m/s, $v_R = 100$ m/s).

A. Time-Variant Delay PSD

By imposing the time-dependent mean powers and delays of clusters, the cluster delay PSD can be acquired. Moreover, using the mean delays of rays within one cluster and the corresponding powers of rays, the ray delay PSD can also be exhibited as in Fig. 5. From this figure, we can observe the profile of power along with the delay at different time instants. The delay PSDs are different at time instants $t = 2$ s and $t = 4$ s.

B. Time-Variant ACF

Based on the massive MIMO and mmWave HST channel model, the non-stationarity of the proposed channel model can be described effectively. By adopting $\Delta x_T = 0$, $\Delta x_R = 0$, and $\Delta f = 0$, the ACF of theoretical model can be obtained. Then, using the MEA method, the ACF of simulation model can be acquired. The comparisons of time ACFs of theoretical model

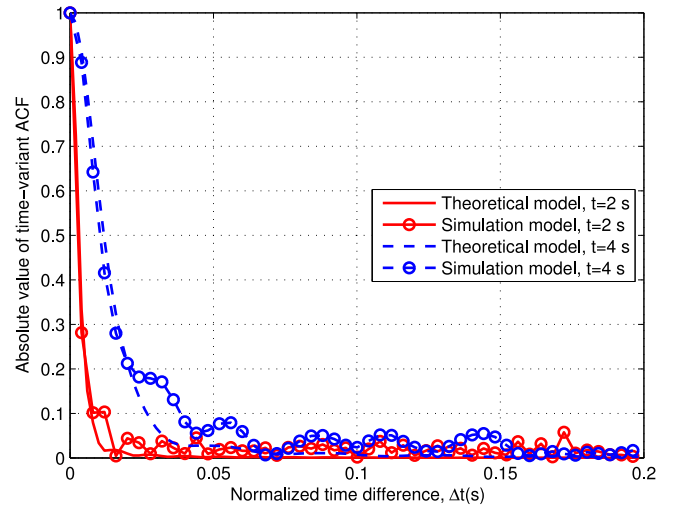


Fig. 6. The time-variant ACFs of the theoretical model and simulation model ($f_c = 58$ GHz, $D_{p_n, m_n}^T(t_0) = 50$ m, $D_{q_n, m_n}^R(t_0) = 100$ m, $\lambda_G = 80$ m, $\lambda_R = 4$ m, $v_{n,A} = 30$ m/s, $v_{n,Z} = 30$ m/s, $v_R = 100$ m/s).

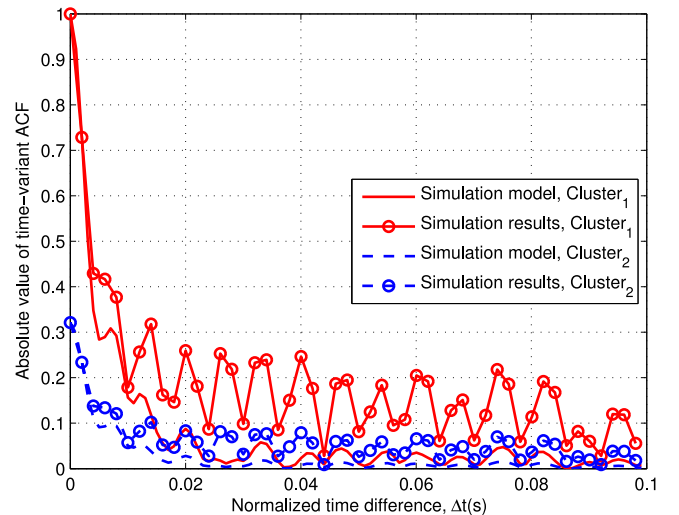


Fig. 7. The comparison of time-variant ACFs of simulation model and simulation results ($f_c = 58$ GHz, $D_{p_n, m_n}^T(t_0) = 50$ m, $D_{q_n, m_n}^R(t_0) = 100$ m, $\lambda_G = 80$ m, $\lambda_R = 4$ m, $v_{n,A} = 30$ m/s, $v_{n,Z} = 30$ m/s, $v_R = 100$ m/s).

and simulation model are illustrated in Fig. 6. From this figure, we can see that the simulation model provides a good approximation of the theoretical model. Moreover, the absolute values of ACFs at different time instants, i.e., $t = 2$ s and $t = 4$ s can be obtained. At different time instants, there are different ACFs of proposed HST channel model, which demonstrates that the proposed model can capture the non-stationarity of channel. To validate the accuracy of the proposed HST channel model, the ACFs of simulation model and the corresponding simulation results for both $Cluster_1$ and $Cluster_2$ are compared in Fig. 7. It should be noted that both of ACFs are normalized by $Cluster_1$. It can be observed from Fig. 7 that the simulation model can match well with the simulation results. The simulation model align well with simulation results for $Cluster_1$ and $Cluster_2$ cases.

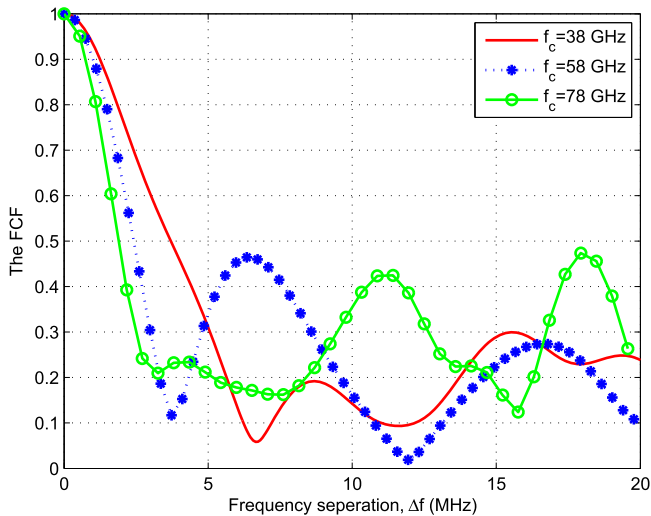


Fig. 8. The FCFs of the proposed simulation channel model at different frequencies f_c ($D_{pn,m_n}^T(t_0) = 50$ m, $D_{qn,m_n}^R(t_0) = 100$ m, $\lambda_G = 80$ m, $\lambda_R = 4$ m, $v_R = 100$ m/s).

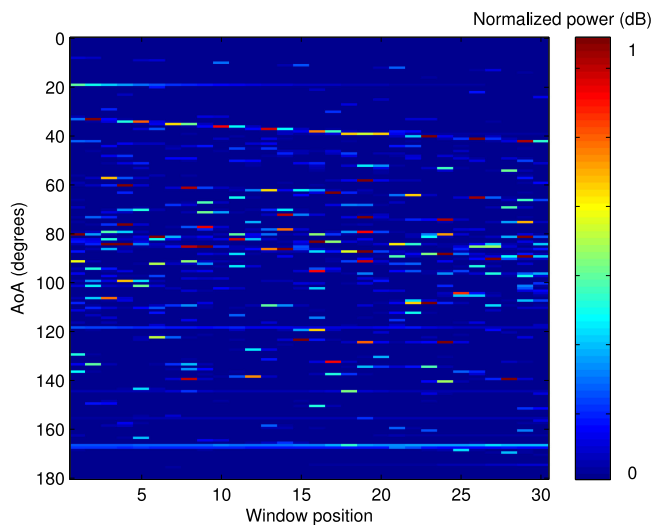


Fig. 9. The angular PSD of the proposed simulation channel model ($D_{pn,m_n}^T(t_0) = 50$ m, $D_{qn,m_n}^R(t_0) = 100$ m, $v_{n,A} = 30$ m/s, $v_{n,Z} = 30$ m/s, $v_R = 100$ m/s).

C. The FCF

The absolute values of the FCFs of the 3D massive MIMO and mmWave HST channel model are illustrated in Fig. 8. From this figure, we can notice that the FCFs are different at $f_c = 38$ GHz, 58 GHz, and 78 GHz, which show the frequency non-stationarities of the proposed channel model.

D. Angular PSD

The simulated normalized angular PSD at the moving Rx of the 3D massive MIMO and mmWave channel model is illustrated in Fig. 9. It can be observed that the clusters show appearance and disappearance properties on the massive MIMO array axis, which exhibit the clusters birth and death from space

domain. Moreover, the angular shifts can be obtained, which result from the spherical wavefront effect of massive MIMO.

V. CONCLUSIONS

In this paper, a novel 3D space-time-frequency non-stationary mmWave massive MIMO theoretical channel model for 5G HST communication channels has been proposed. The corresponding simulation channel model has been developed using the MEA. Based on the proposed theoretical and simulation models, their statistical properties have been investigated, including time-variant ACF, space CCF, delay PSD, angular PSD, and FCF. Numerical and simulation results have shown that the statistical properties of the simulation model can match well with those of the theoretical model. Moreover, due to the movements of clusters and MRS, the statistical properties experience different behaviors at different time instants, which has demonstrated that our proposed models can mimic the non-stationarity of HST channels. By introducing the model parameters in space, time, and frequency domains, the joint space-time-frequency non-stationarity of the proposed HST channel model has been investigated.

REFERENCES

- [1] C.-X. Wang *et al.*, "Cellular architecture and key technologies for 5G wireless communication networks," *IEEE Commun. Mag.*, vol. 52, no. 2, pp. 122–130, Feb. 2014.
- [2] C.-X. Wang, A. Ghazal, B. Ai, P. Fan, and Y. Liu, "Channel measurements and models for high-speed train communication systems: A survey," *IEEE Commun. Surv. Tut.*, vol. 18, no. 2, pp. 974–987, Apr.–Jun. 2016.
- [3] K. Guan *et al.*, "On millimeter wave and THz mobile radio channel for smart rail mobility," *IEEE Trans. Veh. Technol.*, vol. 66, no. 7, pp. 3349–3516, Jul. 2017.
- [4] S. Wu, C.-X. Wang, H. Haas, H. Aggoune, M. M. Alwakeel, and B. Ai, "A non-stationary wideband channel model for massive MIMO communication systems," *IEEE Trans. Wireless Commun.*, vol. 14, no. 3, pp. 1434–1446, Mar. 2015.
- [5] J. Huang, C.-X. Wang, R. Feng, J. Sun, W. Zhang, and Y. Yang, "Multi-frequency mmWave massive MIMO channel measurements and characterization for 5G wireless communication systems," *IEEE J. Sel. Areas Commun.*, vol. 35, no. 7, pp. 1591–1605, Jul. 2017.
- [6] B. Ai *et al.*, "Challenges toward wireless communications for high-speed railway," *IEEE Trans. Intell. Transp. Syst.*, vol. 15, no. 5, pp. 2143–2158, Oct. 2014.
- [7] S. Wu, C.-X. Wang, H. Aggoune, M. M. Alwakeel, and X. You, "A general 3D non-stationary 5G wireless channel model," *IEEE Trans. Commun.*, vol. 66, no. 7, pp. 3065–3078, Jul. 2018.
- [8] C.-X. Wang, J. Bian, J. Sun, W. Zhang, and M. Zhang, "A survey of 5G channel measurements and models," *IEEE Commun. Surv. Tut.*, vol. 20, no. 4, pp. 3142–3168, Fourth Quarter 2018.
- [9] K. Guan, Z. Zhong, B. Ai, and T. Kürner, "Propagation measurements and analysis for train stations of high-speed railway at 930 mHz," *IEEE Trans. Veh. Technol.*, vol. 63, no. 8, pp. 3349–3516, Oct. 2014.
- [10] S. Knorz, M. A. Baldauf, T. Fugen, and W. Wiesbeck, "Channel analysis for an OFDM-MISO train communications system using different antennas," in *Proc. IEEE 66th Veh. Technol. Conf.*, Baltimore, MD, USA, Oct. 2007, pp. 809–813.
- [11] D. J. Cichon, T. Becker, and W. Wiesbeck, "Determination of time-variant radio links in high-speed train tunnels by ray optical modeling," in *Proc. IEEE Antennas Propag. Soc. Int. Symp.*, Newport Beach, CA, USA, Jun. 1995, pp. 508–511.
- [12] D. J. Cichon, T. Zwick, and W. Wiesbeck, "Ray optical modeling of wireless communications in high-speed railway tunnels," in *Proc. IEEE Veh. Technol. Conf.*, Atlanta, GA, USA, May 1996, pp. 546–550.
- [13] B. Chen, Z. Zhong, and B. Ai, "Stationarity intervals of time-variant channel in high speed railway scenario," *China Commun.*, vol. 9, no. 8, pp. 64–70, Aug. 2012.

- [14] A. Ghazal, C.-X. Wang, B. Ai, D. Yuan, and H. Haas, "A non-stationary wideband MIMO channel model for high-mobility intelligent transportation systems," *IEEE Trans. Intell. Transp. Syst.*, vol. 16, no. 2, pp. 885–897, Apr. 2015.
- [15] A. Ghazal *et al.*, "A non-stationary IMT-A MIMO channel model for high-mobility wireless communication systems," *IEEE Trans. Wireless Commun.*, vol. 16, no. 4, pp. 2057–2068, Apr. 2017.
- [16] J. Bian *et al.*, "A WINNER+ based 3D non-stationary wideband MIMO channel model," *IEEE Trans. Wireless Commun.*, vol. 17, no. 3, pp. 1755–1767, Mar. 2018.
- [17] Y. Liu, C.-X. Wang, C. F. Lopez, and X. Ge, "3D non-stationary wideband circular tunnel channel models for high-speed train wireless communication systems," *Sci. China Inf. Sci.*, vol. 60, no. 8, pp. 1–13, Aug. 2017.
- [18] Y. Liu, A. Ghazal, C.-X. Wang, X. Ge, Y. Yang, and Y. Zhang, "Channel measurements and models for high-speed train wireless communication systems in tunnel scenarios: A survey," *Sci. China Inf. Sci.*, vol. 60, no. 8, pp. 1–17, Oct. 2017.
- [19] X. Yin, X. Cai, X. Cheng, J. Chen, and M. Tian, "Empirical geometry based random-cluster model for high-speed-train channels in UMTS networks," *IEEE Trans. Intell. Transp. Syst.*, vol. 16, no. 5, pp. 2850–2861, Oct. 2015.
- [20] Y. Cui and X. Fang, "Performance analysis of massive spatial modulation MIMO in high-speed railway," *IEEE Trans. Veh. Technol.*, vol. 65, no. 11, pp. 8925–8932, Nov. 2016.
- [21] H. Song, X. Fang, and Y. Fang, "Millimeter-wave network architectures for future high-speed railway communications: Challenges and solutions," *IEEE Wireless Commun.*, vol. 23, no. 6, pp. 114–122, Dec. 2016.
- [22] L. Liu *et al.*, "The COST 2100 mIMO channel model," *IEEE Wireless Commun.*, vol. 19, no. 6, pp. 92–99, Dec. 2012.
- [23] S. Jaeckel, L. Raschkowski, K. Brner, and L. Thiele, "QuaDRiGa: A 3-D multi-cell channel model with time evolution for enabling virtual field trials," *IEEE Trans. Antennas Propag.*, vol. 62, no. 6, pp. 3242–3256, Jun. 2014.
- [24] "3rd generation partnership project, technical specification group radio access network, study on 3D channel model for LTE (Release 12)," 3GPP, Sophia Antipolis Cedex, France, 3GPP TR 36.873, V12.0.0, Jun. 2015.
- [25] "5G channel model for bands up to 100 GHz," Aalto University, Aalto, Finland, v2.0, Mar. 2014.
- [26] S. Wu, C.-X. Wang, H. Aggoune, M. M. Alwakeel, and Y. He, "A non-stationary 3D wideband twin-cluster model for 5G massive MIMO channels," *IEEE J. Sel. Areas Commun.*, vol. 32, no. 6, pp. 1207–1218, Jun. 2014.
- [27] C.-X. Wang, S. Wu, L. Bai, X. You, J. Wang, and C.-L. I, "Recent advances and future challenges for massive MIMO channel measurements and models," (*Invited Paper*) *Sci. China Inf. Sci.*, vol. 59, no. 2, pp. 1–16, Feb. 2016.
- [28] R. C. Qiu, "A study of the ultra-wideband wireless propagation channel and optimum UWB receiver design," *IEEE J. Sel. Areas Commun.*, vol. 20, no. 9, pp. 1628–1637, Dec. 2002.
- [29] R. He *et al.*, "Characterization of quasi-stationarity regions for vehicle-to-vehicle radio channels," *IEEE Trans. Antennas Propag.*, vol. 63, no. 5, pp. 2237–2251, May 2015.
- [30] T. Zwick, C. Fischer, D. Didascalou, and W. Wiesbeck, "A stochastic spatial channel model based on wave-propagation modeling," *IEEE J. Sel. Areas Commun.*, vol. 18, no. 1, pp. 6–15, Jan. 2000.
- [31] K. Pekka, "WINNER II channel models part II radio channel measurement and analysis results," IST-4-027756, WINNER II D1.1.2, v1.0, Sep. 2007.



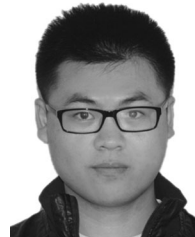
Yu Liu received the B.Sc. and M.Eng. degrees in communication and information systems from Qufu Normal University, China, in 2010 and 2013, respectively, and the Ph.D. degree in communication and information systems from Shandong University, China, in 2017. Since August 2017, she has been a Postdoctoral Research Associate with the School of Information Science and Engineering, Shandong University. Her main research interests include non-stationary wireless MIMO channel modeling, high-speed train wireless propagation characterization and modeling, and channel modeling for special scenarios.



Cheng-Xiang Wang (S'01–M'05–SM'08–F'17) received the B.Sc. and M.Eng. degrees in communication and information systems from Shandong University, Jinan, China, in 1997 and 2000, respectively, and the Ph.D. degree in wireless communications from Aalborg University, Aalborg, Denmark, in 2004.

He was a Research Assistant with the Hamburg University of Technology, Hamburg, Germany, from 2000 to 2001, a Visiting Researcher with Siemens AG Mobile Phones, Munich, Germany, in 2004, and a Research Fellow with the University of Agder, Grimstad, Norway, from 2001 to 2005. Since 2005, he has been with Heriot-Watt University, Edinburgh, U.K., where he was promoted to a Professor in 2011. In 2018, he joined Southeast University, Nanjing, China, as a Professor and Thousand Talent Plan Expert. He has authored and coauthored 2 books, 1 book chapter, and more than 340 papers in refereed journals and conference proceedings. His current research interests include wireless channel modeling and (B)5G wireless communication networks, including green communications, cognitive radio networks, high mobility communication networks, massive MIMO, millimetre wave communications, and visible light communications.

Dr. Wang is a Fellow of the IET and HEA, and is recognized as a Web of Science 2017 Highly Cited Researcher. He served or is currently serving as an Editor for nine international journals, including the IEEE TRANSACTIONS ON VEHICULAR TECHNOLOGY since 2011, the IEEE TRANSACTIONS ON COMMUNICATIONS since 2015, and the IEEE TRANSACTIONS ON WIRELESS COMMUNICATIONS from 2007 to 2009. He was the leading Guest Editor for the IEEE JOURNAL ON SELECTED AREAS IN COMMUNICATIONS (Special Issue on Vehicular Communications and Networks). He is also a Guest Editor for the IEEE JOURNAL ON SELECTED AREAS IN COMMUNICATIONS (Special Issue on Spectrum and Energy Efficient Design of Wireless Communication Networks and Special Issue on Airborne Communication Networks), and the IEEE TRANSACTIONS ON BIG DATA, (Special Issue on Wireless Big Data). He served or is serving as a TPC Member, TPC Chair, and General Chair of more than 80 international conferences. He received nine Best Paper Awards from the IEEE Globecom 2010, the IEEE ICCT 2011, ITST 2012, the IEEE VTC 2013, IWCMC 2015, IWCMC 2016, the IEEE/CIC ICC 2016, and the WPMC 2016.



Jie Huang received the B.Sc. degree in information engineering from the Xidian University, Xi'an, China, in 2013, and the Ph.D. degree in communication and information systems from Shandong University, Jinan, China, in 2018. Since August 2018, he has been a Postdoctoral Research Associate with the Mobile Communications Research Laboratory, Southeast University, Nanjing, China. His current research interests include millimeter wave and massive MIMO channel measurements, parameter estimation, channel modeling, wireless big data, and 5G wireless communications.



Jian Sun (M'08) received the Ph.D. degree from Zhejiang University, Hangzhou, China, in March 2005. Since July 2005, he has been a Lecturer with the School of Information Science and Engineering, Shandong University, Jinan, China. In 2011, he was a visiting scholar with Heriot-Watt University, Edinburgh, U.K., supported by U.K.–China Science Bridges: R&D on (B)4G Wireless Mobile Communications (UC4G) project. His research interests include signal processing for wireless communications, channel sounding and modeling, propagation

measurement and parameter extraction, MIMO, and multicarrier transmission systems design and implementation.



Wensheng Zhang (S'08–M'11) received the M.Sc. degree in communication and information systems from Shandong University, Jinan, China, in 2005, and the Ph.D. degree in communication engineering from Keio University, Tokyo, Japan, in 2011. From 2005 to 2007, he was a Lecturer with the School of Communication, Shandong Normal University, Jinan, China. In 2011, he was a Visiting Researcher with Oulu University, Oulu, Finland. Since 2012, he has been a Lecturer with the School of Information Science and Engineering, Shandong University,

Jinan, China, where he was promoted to an Associate Professor in 2016. His research interests include random matrix theory and big data analysis, visible light communication networks, intelligent wireless communication systems, and 5G wireless communications.